Single Frequency Approximation of Volume Conductor Models for Deep Brain Stimulation using Equivalent Circuits

Christian Schmidt and Ursula van Rienen
Institute of General Electrical Engineering, University of Rostock, Albert-Einstein-Str. 2, 18059 Rostock, Germany

Keywords: Deep Brain Stimulation, Finite Element Method, Fourier Transform.

Abstract: The objective of this study was to investigate the role of frequency-dependent material properties on the voltage response and neural activation in a volume conductor model for deep brain stimulation (DBS). A finite element model of the brain was developed comprising tissue heterogeneity of gray matter, white matter, and cerebrospinal fluid, which was derived from magnetic resonance images of the SRI24 multi-channel brain atlas. A model of the Medtronic DBS 3387 lead surrounded by an encapsulation layer was positioned in the subthalamic nucleus (STN). The frequency-dependent properties of brain tissue and their single-frequency approximations were modelled as voltage- and current-controlled equivalent circuits. The frequency of best approximation, for which the pulse deviation between the single-frequency and frequency-dependent voltage response were minimal, was computed in a frequency range between 130 Hz and 1.3 MHz. Single-frequency approximations of the DBS pulses and the resulting volume of tissue activated (VTA) were found to be in good agreement with the pulses and VTAs obtained from the frequency-dependent solution. Single-frequency approximations were computed by combining finite element method with equivalent circuits. This method allows a fast computation of the time-dependent voltage response in the proximity of the stimulated target by requiring only one finite element computation.

1 INTRODUCTION

Deep brain stimulation (DBS) is a neurosurgical method to treat symptoms of motor disorders such as Parkinson's disease (PD), essential tremor and dystonia and has emerged as an effective treatment (Uc and Follet, 2007). Although the method has become a common procedure in the clinical field of PD, the fundamental mechanisms of DBS remain uncertain (Montgomery Jr. and Gale, 2008). Computational models can help to gain knowledge about these mechanisms by predicting field distributions and the neural response in stimulated brain areas. The field distribution which directly affects the neural response, and therefore the stimulation benefit, is dependent on a variety of factors. These factors concern, amongst others, the model geometry (Walckiers et al., 2010), the frequency-dependent electrical properties of brain tissue (Grant and Lowery, 2010), the effects occurring at the electrode-tissue interface (Cantrell et al., 2008) and the reaction of the body to the electrode, resulting in the growth of a so-called encapsulation layer around the electrode (Yousif and Liu, 2009).

The electric properties of biological tissue show a frequency dependence over a wide spectrum (Gabriel et al., 1996). To investigate the effect of dispersive tissue in DBS an appropriate formulation of the underlying physics has to be made. Therefore, an electroquasistatic (EQS) formulation was used, which applies for the time-harmonic electric fields generated in the proximity of the stimulated target by the applied DBS pulse (van Rienen, 2000). In a preliminary study it was concluded that dispersive effects of the electrical tissue properties could be neglected under current-controlled stimulation for appropriate conductivity values (Bossetti et al., 2008). Results were obtained by comparing a single frequency solution comprising a fixed conductivity value with the dispersive solution in an homogeneous finite element model. These results were expanded in a following study by using an improved anatomically head model and comparing dispersive solutions with single frequency solutions under current- and voltage-controlled stimulation (Grant and Lowery, 2010). However, the brain tissue remained homogeneous and the deviation between the single frequency and dispersive solutions of the model were investigated only at 100 Hz, 1 kHz, and 1 MHz. In the mentioned study, the computation

Schmidt C. and van Rienen U..
Single Frequency Approximation of Volume Conductor Models for Deep Brain Stimulation using Equivalent Circuits.
DOI: 10.5220/0004223700380047
In *Proceedings of the International Conference on Bio-inspired Systems and Signal Processing* (BIOSIGNALS-2013), pages 38-47
ISBN: 978-989-8565-36-5

of the voltage response at a position in the proximity of the stimulated target was carried out using the so-called Fourier finite element method, in which the required transfer function is determined by the electric potential at this position for each frequency component of the DBS pulse (Butson and McIntyre, 2005). Since a precise modelling of a square-wave pulse with a frequency of 130 Hz and a pulse width of 60 µs, as used in DBS therapy, requires several thousand Fourier components, the computation of the transfer function even for an approximation at a single frequency becomes rather computationally expensive.

We propose the use of equivalent circuits for the approximation of the transfer function, in which the electrical properties of the brain model are determined by the resistance and capacitance of the volume conductor model. The resistance and capacitance can be computed for the single-frequency solution by only one evaluation of the brain model, which allows a time-efficient computation of the voltage response for a single-frequency solution, and, therefore, facilitates the comparison of the single-frequency solutions with the frequency-dependent solution across a wide range of frequencies. To date, the influence of the interaction of the different dispersive brain tissue types on the approximation of the dispersive solution by a solution in which the electrical properties are estimated at a single frequency across a wide range of frequencies remains unquantified. Therefore, the objective of this study was to investigate the influence of frequency-dependent material properties of brain tissue on the voltage response and neural activation for 200 different frequencies across a range from 130 Hz to 1.3 MHz in an heterogeneous and anatomically head model using an equivalent circuit approach.

2 METHODS

2.1 Finite Element Model

The geometry used for the brain consists of an idealized human brain modelled as an ellipsoid (Fig. 1). The spatial dimensions of the brain model were derived from the the SRI24 multi-channel brain atlas which is a standard atlas of the human brain based on magnetic resonance images (Rohlfing et al., 2008). The atlas comprises averaged 3 T MRI images and tissue segmentations with a voxel size of 1 mm^3 of 24 volunteers spanning from 19 to 84 years old. The brain tissue is segmented into white matter, gray matter and cerebrospinal fluid. The position of the STN was determined using a brain atlas and comparing axial, coronal and sagittal slices of the T1-weighted

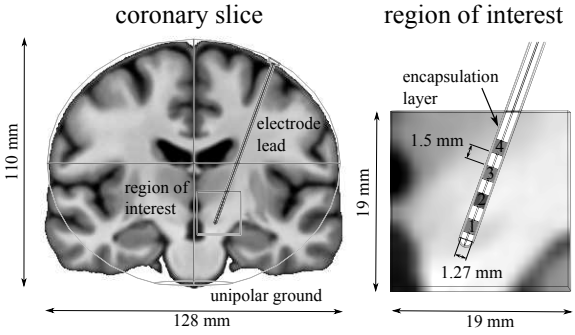

Figure 1: Coronary slice of the model geometry. T1 MRI data of the SRI24 multi-channel brain atlas is shown in the background.

MRI data with the atlas (Kretschmann and Weinrich, 1991).

A model of the Medtronic 3387 DBS electrode, comprising 4 equidistantly spaced platin-iridium contacts, was subtracted from the model preserving the insulation and contact surface information for the application of boundary conditions. The electrode lead was implemented in the model with the second electrode contact positioned in the centre of the stimulated target. An encapsulation layer with a thickness of 0.2 mm was incorporated around the electrode. To apply unipolar electrode configurations, the bottom of the ellipsoid was modelled as a plane circle with a radius of 22 mm. The electrode tip and the stimulated target was surrounded by a cube-shaped region of interest (ROI) with an edge length of 19 mm, which had a finer mesh density than the remaining brain model. The segmented MRI dataset was preprocessed in MATLAB to reformat the data to an right-handed coordinate system, which was required by the finite element software. A more detailed description of the model geometry can be found in a preliminary study (Schmidt and van Rienen, 2012).

2.2 Mesh Generation

The model was meshed with tetrahedral elements using the Delaunay method. The triangular mesh of the electrode contact surfaces were manually refined until the alteration of the integral of the current density over the surface area of the active electrode was below 1%, which was obtained for a maximum element length of 0.1 mm. To avoid disconformity between the tetrahedral mesh and the hexahedral elements of the MRI data, the mesh within the ROI was set to a maximum element length of 0.5 mm. The resulting mesh of the brain model contained out of about 1.4 million elements.

2.3 Electrical Properties of Tissue

The conductivity and relative permittivity of biological tissues, both, show a frequency dependence which can be described by different dispersion regions each expressed as a Cole-Cole term. The conductivity and relative permittivity of gray matter, white matter, and cerebrospinal fluid was computed by a 4 Cole-Cole term expression using the data of an experimental study (Gabriel et al., 1996). The electrical tissue properties of the encapsulation layer around the implant vary over time from an acute phase immediately after surgery to a chronic phase after some weeks due to cell growth in the layer. This results in an increase of the resistivity compared to that of the brain tissue (Grill and Mortimer, 1994). To model the longterm effects of DBS, the encapsulation layer was modelled in the chronic phase by using the halved conductivity value of gray matter (Butson and McIntyre, 2005) and the relative permittivity of brain tissue (Yousif and Liu, 2009).

2.4 Finite Element Computation

The voltage distribution in the proximity of the stimulated target as well as the resistance R and capacitance C of the brain model was computed using finite element method. Therefore, the electro-quasistatic (EQS) formulation

$$\nabla\left[\left(\sigma(\omega)+\mathrm{j}\omega\varepsilon_0\varepsilon_r(\omega)\right)\nabla\phi\right]=0\,, \qquad (1)$$

with the electric potential ϕ, the imaginary unit j, the angular frequency ω, the frequency-dependent conductivity $\sigma(\omega)$, the frequency-dependent relative permittivity $\varepsilon_r(\omega)$ and the electric field constant $\varepsilon_0 \approx 8.854\cdot10^{-12}\,\mathrm{A\,s\,/\,V\,m}$, was applied to the brain model, which is a valid approximation of the electromagnetic wave equation for bio-electrical applications in the human brain (Bossetti et al., 2008). The exterior boundary of the idealized brain was modelled as insulation using Neumann boundary condition. To apply voltage-controlled or current-controlled stimulation, the surface of the active electrode contact was set to a constant potential or constant normal current density, respectively. In both cases, the ground electrode located at the bottom of the brain model was set to a constant potential of $\phi_0 = 0\,\mathrm{V}$. The remaining electrode contacts were set to floating potential, i.e. no net current flow occurring through the contact surfaces. The finite element computations were performed with the commercial software COMSOL Multiphysics. Quadratic shape functions were used. The assembled linear system of equations was solved using generalized minimal residual method (GMRES) with a geometric multigrid as preconditioner. Iteration was stopped when the 2-norm of the residual was below $1\cdot10^{-6}$. The electric potential ϕ, the resistance R, and the capacitance C are determined for 50 frequencies in each decade between 130 Hz and 1.3 MHz resulting in 200 frequencies. The frequency-dependent resistance $R(\omega)$ and capacitance $C(\omega)$ were computed using the integral of the current density over the surface area of the active electrode contact with the expressions

$$R(\omega)=\frac{U}{\Re(I(\omega))}\,,\quad C(\omega)=\frac{\Im(I(\omega))}{\omega U} \qquad (2)$$

with the voltage $U=\phi_1-\phi_0$, and the real part $\Re(I)$ and the imaginary part $\Im(I)$ of the current, while the surface of the active electrode contact was set to a constant potential of $\phi_1 = 1\,\mathrm{V}$.

2.5 Waveform Computation

The DBS pulses applied to the DBS electrode in this study are commonly used in DBS therapy and consist of a monophasic square-wave signal with a pulse duration of d_p =60 µs, a frequency of f =130 Hz and a cathodic amplitude of A_{vc} =3 V for voltage-controlled stimulation and A_{cc} =1.5 mA for current-controlled stimulation. The DBS pulses $y(t)$ are modelled in time-domain and transformed into frequency-domain using a fast Fourier transform (FFT) with a sampling rate of 1 MHz. Since an ideal square-wave signal has, by definition, points of discontinuity, the Fourier synthesis of the finite Fourier components X_{k} of the signal can result in an overshooting at these points, which is in the order of 9 % for a square-wave signal, if the Fourier synthesis is truncated. To avoid this effect, the square-wave pulses were smoothed using the function

$$y(t)=\frac{A}{2}\left\{1+\tanh\left[a\left(\frac{d_{\mathrm{p}}}{2}-|t|\right)\right]\right\}, \qquad (3)$$

with the slope coefficient a. The smoothing of the signal reduces the influence of high frequency components, and therefore the overshooting, but could also influence the effect of tissue capacitance. To investigate this effect, the DBS pulses were also modelled as ideal square-wave signals by a step function using the same pulse parameters. The slope coefficient was set to $1\cdot10^{6}$, which resulted in a cut-off frequency of 151 kHz (Fig. 2). At a cut-off frequency of 151 kHz the square-wave signal is significantly smoothed, reducing the overshoot below 0.1 %, while its overall shape is preserved. To receive the voltage response in the proximity of the stimulated target at a location $\boldsymbol{r}$, the Fourier components X_{k} were scaled and phase shifted by the transfer function $T(\omega)$ obtained

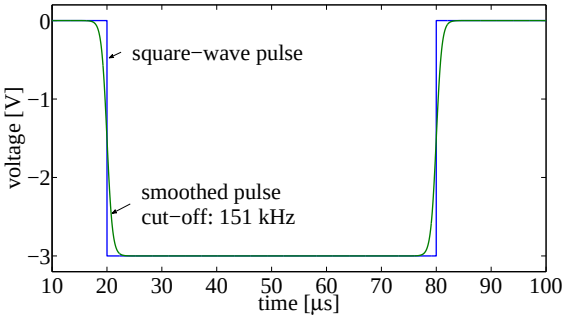

Figure 2: Voltage-controlled pulse modelled as a square-wave signal (blue) and as a smoothed signal with a cut-off frequency of 151 kHz (green).

from the finite element computation by multiplying the Fourier components X_k component for component with the transfer function $T(\omega_k)$ at the corresponding frequency ω_k (Butson and McIntyre, 2005). In the proposed method, this transfer function is approximated using an equivalent circuit comprising the parallel RC circuit from the finite element model and a constant phase element CPE, which models the electrode-tissue-interface. The impedance Z_{CPE} of this interface is expressed by

$$Z_{CPE} = \frac{K}{A_s(j\omega)^\beta} \tag{4}$$

where $K = 1.51\,\Omega\,m^2\,s^{-\beta}$, $\beta = 0.91$, and the active electrode contact surface area A_s =5.98 µm^2 (Cantrell et al., 2008). *In vivo* and *in vitro* measurements for current controlled DBS stimulation showed a strongly non-linear dependence of the double layer on the stimulus amplitude for frequencies below 100 Hz, but not at high frequencies above 100 Hz (Wei and Grill, 2009). For the used DBS pulses, the spectral energy density below 130 Hz contains only about 1.5 % of the total spectral energy density. Therefore, it is assumed in this study, that the electrode-tissue-interface can be modelled by the linear constant phase element.

2.5.1 Voltage-controlled Stimulation

The single frequency approximation of the transfer function T_{vc} for the voltage-controlled case was obtained by using a constant potential boundary condition on the surface of the active electrode contact, resulting in a total voltage of $A_{vc,FEM}$ =1 V in the finite element model. By using the equation for a frequency-dependent voltage divider, the transfer function T_{vc} and the scaled Fourier components $X_{k,vc}$ at a position $\boldsymbol{r}$ are expressed by

$$T_{vc}(\omega_k) = \left[1 + \left(\frac{1}{R(\omega_s)} + j\omega_k C(\omega_s)\right) Z_{CPE}(\omega_k)\right]^{-1} \tag{5}$$

$$X_{k,vc}(\omega_s) = \frac{T_{vc}(\omega_k)}{|T_{vc}(\omega_s)|} \cdot \frac{|\phi(\boldsymbol{r},\omega_s)|}{|A_{vc,FEM}|} X_k\,. \tag{6}$$

Since the constant phase element is not incorporated into the finite element computation, the frequency-dependent transfer function for the voltage-controlled case is obtained by multiplying the transfer function T_{vc} component for component with the frequency-dependent voltage $\phi(\boldsymbol{r},\omega)$ of the finite element computation.

2.5.2 Current-controlled Stimulation

For current-controlled stimulation, the constant phase element is negligible, since capacitive and dispersive effects dominate the waveform shape (Grant and Lowery, 2010). Therefore, the transfer function T_{cc} for the current-controlled case is only dependent on the resistance R and capacitance C of the finite element model. For the computation of the voltage distribution $\phi(\boldsymbol{r},\omega_s)$, a normal current density boundary condition was set on the surface of the active electrode contact, resulting in a total current of $A_{cc,FEM}$ =1.5 mA in the finite element model. The resulting transfer function T_{cc} and the scaled Fourier components $X_{k,cc}$ at a position $\boldsymbol{r}$ are expressed by

$$T_{cc}(\omega_k) = \left(\frac{1}{R(\omega_s)} + j\omega_k C(\omega_s)\right)^{-1} \tag{7}$$

$$X_{k,cc}(\omega_s) = \frac{T_{cc}(\omega_k)}{|T_{cc}(\omega_s)|} \cdot \frac{|\phi(\boldsymbol{r},\omega_s)|}{|A_{cc,FEM}|} X_k\,. \tag{8}$$

The transfer functions obtained from the finite element computations at the 200 frequencies in the frequency range between 130 Hz and 1.3 MHz were linearly interpolated on the FFT frequency spectrum of the DBS pulses. The voltage responses derived from the single-frequency approximation using the equivalent circuit models for voltage- and current-controlled stimulation were compared with the voltage responses derived from the frequency-dependent solutions at radial distances between 0.5 mm and 5 mm of the active electrode contact.

2.6 Volume of Tissue Activated

The effect of the single frequency approximation of the voltage response in the proximity of the electrode contact on the neural activation was investigated using

a myelinated axon cable model described by McIntyre *et al.* (McIntyre et al., 2002). The axon model has a diameter of 5.7 μm and includes 21 nodes of Ranvier, paranodal and internodal segments as well as the myelin sheath. At each node, the time dependent voltage response was computed and used to determine the threshold voltage V_t using NEURON (7.2, http://www.neuron.yale.edu). 100 axons were aligned perpendicular to the coronary plane in a rectangular 10×10 grid with a spacing of 0.5 mm parallel and perpendicular to the electrode axis. The grid was positioned caudal and centered to the active electrode contact. The minimum stimulus amplitude necessary to elicit action potential propagation in each axon was determined using Brent's method, as implemented in the SciPy optimisation library (Jones et al., 2001). For the stimulus of the applied pulses, the computed threshold voltages in the grid were approximated by a fourth order polynomial $f(x)$ using least squares fit, where x is the distance to the electrode centre. The volume of tissue activated (VTA) was then computed with disk integration using the roots of $P(y)$ as the interval boundaries.

3 RESULTS

The proposed method requires that the voltage response at different locations can be computed by using the same transfer function scaled by the voltage at these locations. Therefore, the resulting voltage responses at different locations should equal each other except a scaling factor of their amplitude. To investigate the validity of this requirement in the proximity of the stimulated target, the normalized voltage responses and transfer functions for a current-controlled square-wave and smoothed stimulus in a distance of 0.5 mm to 5 mm of the active electrode contact were compared for a solution, in which the values of the electrical properties of brain tissue were determined at a frequency of 1 kHz. The deviation between the root mean square (RMS) of the normalized transfer function is below 0.4 % with respect to the RMS at a distance of 5 mm (Fig. 3). The same behaviour as for the deviation of the transfer function can be observed for the normalized square-wave voltage response at the different distances from the active electrode contact. This deviation decreased to below 0.04 % for the smoothed voltage response, which is a result of the lesser spectral energy density in the higher frequency components of the smoothed DBS pulse compared to the square-wave DBS pulse. Regarding the observed deviations of the transfer function, and the square-wave as well as smoothed

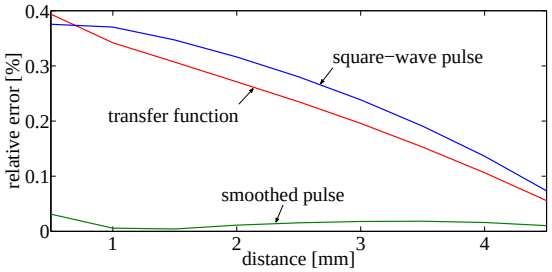

Figure 3: Relative error of the RMS of the normalized transfer functions (red) as well as of the normalized square-wave voltage responses (blue) and smoothed voltage responses (green) for current-controlled stimulation with respect to the values at a distance of 5 mm.

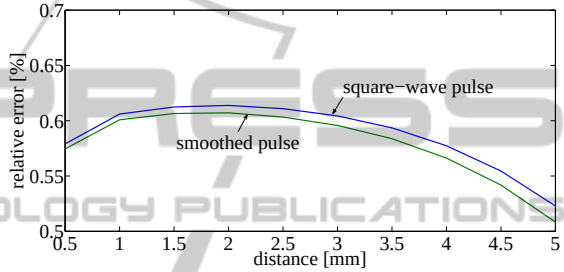

Figure 4: Relative error of the RMS of the single frequency approximation using equivalent circuits for the normalized square-wave voltage responses (blue) and smoothed voltage responses (green) for current-controlled stimulation with respect to the RMS of the voltage responses obtained from the Fourier finite element method.

voltage response, the requirement of a transfer function, which is independent of the location, is considered to be fulfilled.

The square-wave and smoothed voltage response for current-controlled stimulation obtained from the Fourier finite element method were compared with those obtained from the single-frequency approximation using equivalent circuits. The deviation of the RMS of the square-wave voltage responses using equivalent circuits remained between 0.52 % and 0.61 % compared to those obtained from the Fourier finite element method, while a slight decrease of this deviation is noticeable with increasing distance to the active electrode contact (Fig. 4). The deviation of the RMS of the smoothed voltage responses remained between 0.51 % and 0.60 % and showed a similar decrease with increasing distance to the active electrode contact.

The single-frequency approximation of the square-wave and smoothed voltage response for voltage-controlled stimulation was compared with their frequency-dependent solutions for 200 frequencies in a frequency range between 130 Hz and 1.3 MHz at a distance of 1 mm to the active electrode

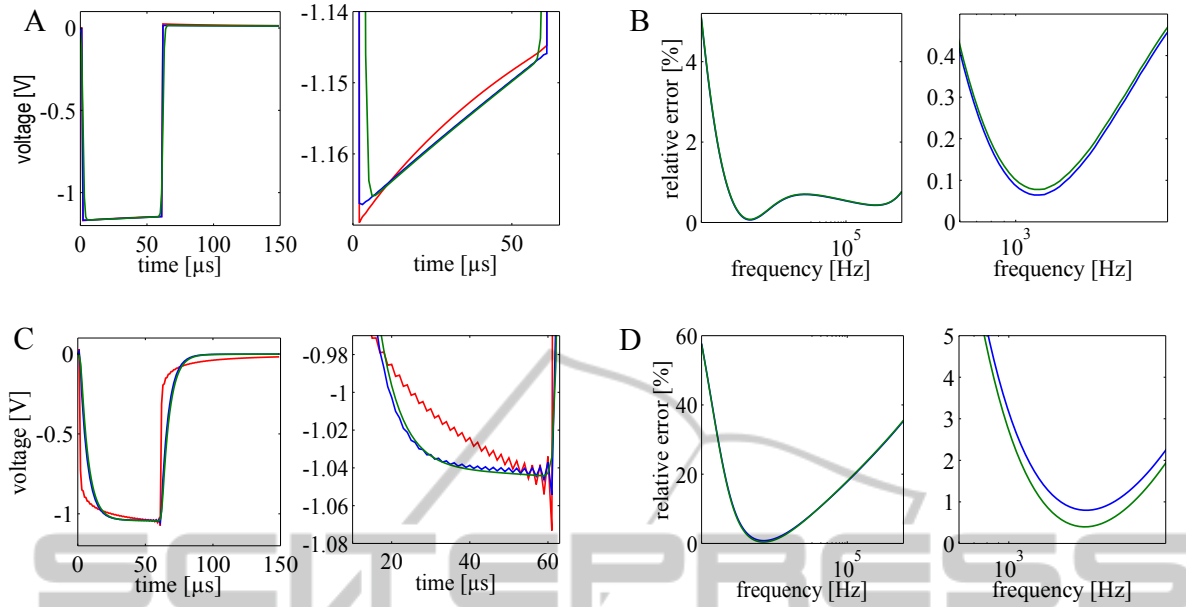

Figure 5: Left: Frequency-dependent voltage response of the square-wave DBS pulse (red) and single-frequency approximation of the square-wave (blue) as well as smoothed DBS pulse (green) at a frequency of 1.2 kHz. Right: Relative error of the RMS of the single-frequency voltage responses with respect to the frequency-dependent voltage responses for the square-wave (blue) and smoothed DBS pulse (green). (A-B) Voltage-controlled stimulation. (C-D) Current-controlled stimulation. On the right of each sub image a magnified section is shown.

contact. The deviation between the single-frequency pulses and the frequency-dependent pulses was minimal at a frequency of approximately 1.2 kHz (Fig. 5B). The relative error of the RMS of the voltage responses at this frequency were 0.06 % for the square-wave DBS pulse and 0.07 % for the smoothed DBS pulse. Despite the smoothing of the slope of the signal, no apparent difference exist between the square-wave and smoothed voltage response in the single-frequency approximation (Fig. 5A). The current-controlled pulse resulting out of the frequency-dependent solution was best approximated by the single frequency solution at a frequency of approximately 2.2 kHz (Fig. 5D) with a relative error of the RMS of 0.8 % for the square-wave DBS pulse and 0.4 % for the smoothed DBS pulse. The deviation of the single-frequency pulses and the frequency-dependent pulses increased in the lower and higher frequency range to 58 % and 36 % for 130 Hz and 1.3 MHz, respectively. These maximal relative errors were much higher than compared to those for voltage-controlled DBS pulses, which were maximal 5.1 % at 130 Hz. The current-controlled voltage responses for the square-wave DBS pulse showed an overshooting of approximately 3 %, which was noticeable for the smoothed DBS pulse (Fig. 5C). The overshooting in a discrete Fourier transform results out of a truncation of high frequency components of the Fourier spectrum of the DBS pulse by the capacitive filtering of the electrical properties of brain tissue. This filtering is decreased for voltage-controlled DBS pulses by the influence of the constant phase element. Therefore, no overshooting is noticeable for voltage-controlled DBS pulses (Fig. 5A).

The influence of the pulse duration of the DBS pulses on the frequency of best approximation was investigated for pulse durations between 60 µs and 120 µs, for which the suppression of symptoms should occur (Medtronic, Inc, 2003). The frequency of best approximation for the current-controlled DBS pulse decreased monotonically from approximately 2.2 kHz to 1.4 kHz within the range of investigated pulse durations, while that for the voltage-controlled DBS pulse increased only slightly from approximately 1.2 kHz to 1.3 kHz (Fig. 6). The relative error of the pulses approximated at a single-frequency remained in each case below 0.8 %.

The volume of tissue activated (VTA) was computed for a stimulus amplitude of 1 V for voltage-controlled stimulation and 0.5 mA for current-controlled stimulation (Fig. 7). The relative error of the VTA computed for the single-frequency square-wave DBS pulses at the best approximation frequency to the VTA computed for the frequency-dependent DBS pulses was below 0.3 % for voltage-controlled stimulation and 5.5 % for current-controlled stimulation (Table 1). This relative

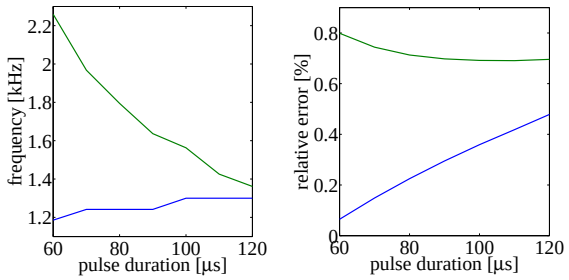

Figure 6: Frequency of best approximation and the corresponding relative error of the RMS of the single-frequency and frequency dependent voltage response for different pulse durations of the DBS pulse. Voltage-controlled DBS pulse (blue). Current-controlled DBS pulse (green).

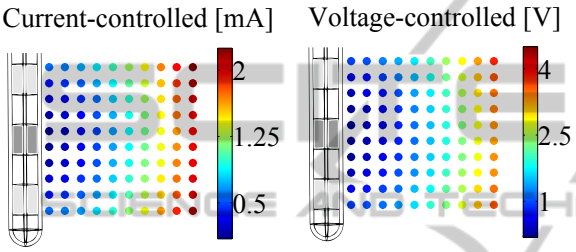

Figure 7: Computed thresholds for the activation of the axons for the frequency-dependent voltage responses scaled by the stimulus amplitude of the current- and voltage-controlled square-wave DBS pulses.

error was similar for the smoothed DBS pulses. However, the VTA for the frequency-dependent DBS pulses varied by 4.2 % for voltage-controlled stimulation when smoothed DBS pulses were used instead of square-wave DBS pulses. Since no overshooting was noticeable in the voltage-controlled pulses, this variation is presumably caused by the smaller slope of the smoothed DBS pulse. For current-controlled stimulation, this variation decreased to 1.5 %.

4 DISCUSSION

The deviation between the voltage response for voltage- and current-controlled stimulation pulses as well as for a smoothed version of the pulses was investigated in the proximity of the stimulated target. The computation of this deviation was carried out at a representative location in 1 mm distance to the active electrode contact. This was possible, since the normalized transfer function and the resulting voltage responses at different locations within the proximity of the stimulated target were almost constant using the Fourier finite element method (Fig. 3). Furthermore, the voltage responses computed with the proposed finite element method in combination with equivalent circuits were in good agreement with those computed with the Fourier finite element method (Fig. 4). The latter requires the computation of the transfer function with the finite element method for several harmonics of the used DBS pulse, which vary between 513 (Yousif and Liu, 2009) and 2,000 (Grant and Lowery, 2010) finite element computations for a common DBS pulse. Instead, the proposed method allows a fast computation of the voltage-response in models with frequency-independent material properties by only one evaluation of the finite element model plus a minor computational effort in post-processing to compute the transfer function.

The influence of the frequency-dependent electrical properties of brain tissue on the voltage-response was approximated by a finite element model using frequency-independent values of the electrical properties of brain tissue by determining them at a single frequency. The results indicate, that the voltage-responses of the frequency-dependent model is in good agreement with those of a single-frequency model at approximately 1.2 kHz and 2.2 kHz for voltage-controlled and current-controlled stimulation (Fig. 5). These results are in agreement with a preliminary study comparing single-frequency approximations of the voltage response with the frequency-dependent solution for three different frequencies between 100 Hz and 10 kHz, suggesting that an estimation of the material properties at a single frequency may provide an approximation of the frequency-dependent solution (Grant and Lowery, 2010). For current-controlled stimulation, the overall deviation between the single-frequency and frequency-dependent voltage responses was larger than for voltage-controlled stimulation in the observed frequency band of 130 Hz to 1.3 MHz. This effect can be ascribed to the constant phase element, which reduces the influence of the frequency-dependent material properties by scaling the representative impedance in the transfer function. The frequency of best approximation for current- and voltage-controlled stimulation varied slightly between 1.3 kHz and 2.2 kHz for different pulse durations of the DBS pulses (Fig. 6). These frequencies are similar to the frequencies of the first dispersive poles of the used electrical properties in the proximity of the stimulated target, i.e. white matter at 1.3 kHz and gray matter at 1.9 kHz (Gabriel et al., 1996). The results suggest that the major influence of the frequency-dependent electrical properties of the used brain tissue can be found at frequencies near those of the dispersive poles. Therefore, a good guess of the frequencies for the single-frequency approximation could be obtained by investigating the frequency-dependent behaviour of the material prop-

Table 1: Computed volume of tissue activated (VTA) for the frequency-dependent and best approximated single-frequency voltage responses for square-wave and smoothed DBS pulses as well as voltage-controlled and current-controlled stimulation.

DBS pulse	Voltage-controlled VTA [mm^3]	Current-controlled VTA [mm^3]
square-wave, frequency-dependent	60.53	46.48
square-wave, single-frequency	60.60	43.93
smoothed, frequency-dependent	57.96	45.76
smoothed, single-frequency	58.10	43.38

erties in the proximity of the stimulated target, which can be achieved in pre-processing.

The computed VTAs for a stimulus amplitude of 1 V for voltage-controlled stimulation and 0.5 mA for current-controlled stimulation had an extent between 43.93 mm^3 and 60.60 mm^3 (Table 1). The results of this study show a larger influence of the frequency-dependent electrical properties of the tissue for current-controlled stimulation. The voltage response for voltage-controlled stimulation is basically influenced by the capacitive effects of the electrical double layer, while under current-controlled stimulation the capacitive and dispersive effects of the bulk tissue dominate the waveform shape. The latter effect results out of the explicit injection of the inward current to the volume conductor model, leading to a negligible influence of the electrical double layer capacitance on the waveform shape. Therefore, higher deviations of the voltage response and the VTA for current-controlled stimulation were observable, which are in agreement with the results in literature (Butson and McIntyre, 2005). While the extent for current-controlled stimulation was slightly smaller than for voltage controlled stimulation, a similar spatial pattern of the required thresholds for the activation was noticeable (Fig. 7). Compared to the deviations in the voltage response of the single-frequency approximations to the frequency-dependent solutions, the corresponding deviation of the VTAs increased to 0.3 % for voltage-controlled stimulation and 5.5 % for current-controlled stimulation. This small deviations of the VTA are in agreement with a computational study, in which the thresholds for a single frequency approximation were compared with the frequency-dependent solution for a point source (Bossetti et al., 2008). While the extent of the VTA slightly increased for the single-frequency approximation for voltage-controlled stimulation, it decreased in current-controlled stimulation, which can be ascribed to the smaller slope of the voltage-response for the single-frequency approximation (Fig. 5C). The voltage responses obtained from the smoothed DBS pulses of the frequency-dependent solution underestimated the corresponding VTAs for the those obtained from the square-wave DBS pulses by 4.2 % for voltage-controlled stimulation and 1.5 % for current-controlled stimulation. Since no overshooting was noticeable in the voltage responses for voltage-controlled stimulation, this effect is presumably caused by the slight variation of the slope of the smoothed DBS pulses compared to the ideal square-wave DBS pulses. These results suggest that the slope of the DBS pulse is a more important parameter for the determination of neural activation than the effect caused by the overshooting of the voltage responses. To reduce the overshooting while preserving the slope of the square-wave DBS pulse, a better approach could be to use the Lanczos sigma approximation (Lanczos, 1996).

The results of this study are based on various assumptions. The MRI images contain voxel data with a resolution of 1 mm, i.e. the data is aligned in a hexahedral mesh, whereas the finite element model is meshed using tetrahedral elements. This leads to disconformities between the hexahedral data mesh and the tetrahedral finite element mesh. To account for this disconformity, a maximum element length of 0.5 mm for the tetrahedral mesh within the region of interest was chosen. A better approach could be to model the important nuclei explicitly, and incorporate them into the finite element model. However, generating an explicit representation of all tissue areas within the brain is still challenging, since the current resolution of MRI data often demands a manual segmentation and volume mesh generation. The results indicate that heterogeneous tissue properties have only a minor influence on the voltage distribution and neural activation in the proximity of the STN in this study, which is noticeable for the computed thresholds resembling an almost homogeneous spatial distribution (Fig. 7). This minor influence could be based on the segmented MRI data from the digital brain atlas, which did not fully render the basal ganglia nuclei, resulting in areas of white matter which are anatomically consistent with gray matter (Rohlfing et al., 2008). MRI data with a more refined segmentation in the region of interest could improve the rendering of the heterogeneous tissue properties in this area. Since the mesh disconformities at the tissue boundaries have only a local influence on the voltage response in the proximity of the stimulated target, it is assumed that this simplification will not in-

fluence a comparison with *in vivo* practice and that a precise representation of the spatial tissue distribution and reliable values for their material parameters are crucial parameters for computing a realistic VTA. However, sources for reliable measurement data of the frequency-dependent electrical properties of biological tissue are still scarce (Faes et al., 1999). This lack of data can be attributed to the taxing requirements and ethical questions that have to be dealt with during the realization of experimental studies.

The uncertainty in the electrical properties of brain tissue and other factors, such as the anisotropy of brain tissue and the electrode position, can influence the voltage response and VTA. To quantify the influence of these uncertainties on the extend of the VTA, probabilistic methods, such as Monte Carlo simulation or Polynomial Chaos would be necessary. The latter method is based on approximating the probabilistic quantities, such as the voltage response and the VTA, by an expansion on a multi-dimensional orthogonal polynomial basis of random parameters (Xiu, 2010). In this case, the computationally expensive deterministic model is only necessary for the computation of the coefficients of this polynomial expansion. This method is already used in various fields of bio-engineering, such as bio-mechanics (Osnes and Joakim, 2012) and drug concentration (Preston et al., 2009), to investigate the influence of uncertainties in the model parameters. In addition, for problem cases with only a small number of uncertain parameters, it is computationally efficient compared to Monte Carlo simulation (Nobile et al., 2008). However, applications of this method in bio-electrical engineering are still scarce.

The neural activation in this study was investigated by the volume of tissue activated for axons aligned perpendicular to the coronary plane in the proximity of the stimulated target, which is a widely accepted method in modelling studies of DBS (Yousif and Liu, 2009). However, this method simplifies the reality, since the neurons of the STN are presumably not evenly oriented and differ in length. Therefore, the used method used to examine the neural activation could underestimate the actual stimulated volume. However, the proposed technique reduces substantially the computational difficulty of evaluating the VTA in volume conductor models of DBS. The extend of the computed VTA and, therefore, the dependence on the parameters observed in this study, could be validated *in vivo* by comparing the predicted activation of adjacent areas to the stimulated target nucleus, such as the oculomotor nerve, for different stimulation amplitudes and the observable response of a patient at these amplitudes (Butson et al., 2006).

The proposed technique for the efficient computation of the voltage response in the proximity of the stimulated target in combination with a probabilistic method based on the Polynomial Chaos can provide mean values and uncertainty bounds for the simulated probabilistic voltage response and neural activation, which could be supportive in *in vivo* practice, with a reasonable computational expense.

5 CONCLUSIONS

In this study, the applicability of a single-frequency approximation of the voltage response based on the estimation of the electrical properties of brain tissue at a single frequency in a heterogeneous head model was investigated. A hybrid method was implemented, which combines finite element method and equivalent circuits to approximate the transfer function of the model. Instead of the popular Fourier finite element method, which requires the evaluation of several finite element models, the proposed method allows a fast computation of the voltage response for voltage- and current-controlled stimulation by only one evaluation of the finite element model plus a minor computational effort in post-processing. The computed single-frequency approximations of the voltage responses were in good agreement with the voltage responses obtained from the frequency-dependent solutions. Furthermore, the frequencies of best approximation resembled approximately the frequencies of the first dispersive poles of the used brain tissues. The fast computation of the voltage response allows further, more complex, applications such as the sensitivity analysis of uncertain parameters of the model using probabilistic methods.

ACKNOWLEDGEMENTS

The authors are grateful to DFG (German Science Foundation) for funding our project in the Research Training Group 1505/1 ”welisa”. The authors would like to thank Peadar Grant from the School of Electrical, Electronic & Communications Engineering at the University College Dublin for his advice on the volume of tissue activated.

REFERENCES

Bossetti, C. A., Birdno, M. J., and Grill, W. M. (2008). Analysis of the quasi-static approximation for calcu-

lating potentials generated by neural stimulation. *J Neural Eng*, 5:44–53.

Butson, C. R., Cooper, S. E., Henderson, J. M., and McIntyre, C. C. (2006). Predicting the effects of deep brain stimulation with diffusion tensor based electric field models. *Med Image Comput Comput Assist Interv*, 9:429–437.

Butson, C. R. and McIntyre, C. C. (2005). Tissue and electrode capacitance reduce neural activation volumes during deep brain stimulation. *Clin Neurophysiol*, 116:2490–2500.

Cantrell, D. R., Inayat, S., Taflove, A., Ruoff, R. S., and Troy, J. B. (2008). Incorporation of the electrodeelectrolyte interface into finite-element models of metal microelectrodes. *J Neural Eng*, 5:54–67.

Faes, T. J. C., van der Meij, H. A., de Munck, J. C., and Heethaar, R. M. (1999). The electric resistivity of human tissues (100 Hz–10 MHz): a meta-analysis of review. *Physiol Meas*, 20:R1–R10.

Gabriel, S., Lau, R. W., and Gabriel, C. (1996). The dielectric properties of biological tissues: Iii parametric models for the dielectric spectrum of tissues. *Phys Med Biol*, 41:2271–2293.

Grant, P. F. and Lowery, M. M. (2010). Effect of dispersive conductivity and permittivity in volume conductor models of deep brain stimulation. *IEEE T Bio-med Eng*, 57:2386–2393.

Grill, W. M. and Mortimer, J. T. (1994). Electrical properties of implant encapsulation tissue. *Ann Biomed Eng*, 22:23–33.

Jones, E., Oliphant, T., Peterson, P., et al. (2001). SciPy: Open source scientific tools for Python.

Kretschmann, H. J. and Weinrich, W. (1991). *Klinische Neuroanatomie und kranielle Bilddiagnostik*. Georg Thieme Verlag, Stuttgart, 2nd edition.

Lanczos, C. (1996). *Linear Differential Operators*. Siam, Philadelphia.

McIntyre, C. C., Richardson, A. G., and Grill, W. M. (2002). Modeling the excitability of mammalian nerve fibers: Influence of afterpotentials on the recovery cycle. *J Neurophysiol*, 87:995–1006.

Medtronic, Inc (2003). Medtronic DBS: Lead Kit for Deep Brain Stimulation.

Montgomery Jr., E. B. and Gale, J. T. (2008). Mechanisms of action of deep brain stimulation. *Neurosci Behav Rev*, 32:388–407.

Nobile, F., Tempone, R., and Webster, C. G. (2008). A sparse grid stochastic collocation method for partial differential equations with random input data. *SIAM J Numer Anal*, 46(5):2309–2345.

Osnes, H. and Joakim, S. (2012). Uncertainty Analysis of Ventricular Mechanics Using the Probabilistic Collocation Method. *IEEE Trans Biomed Eng*, 59:2171–2179.

Preston, J. S., Tasdizen, T., Terry, C. M., Cheung, A. K., and Robert, M. K. (2009). Using the Stochastic Collocation Method for the Uncertainty Quantification of Drug Concentration Due to Depot Shape Variability. *IEEE Trans Biomed Eng*, 56:609–620.

Rohlfing, T., Zahr, N. M., Sullivan, E. V., and Pfefferbaum, A. (2008). The sri24 multi-channel brain atlas. *Proc Soc Photo Opt Instrum Eng*, 6914:691409.

Schmidt, C. and van Rienen, U. (2012). Modeling the Field Distribution in Deep Brain Stimulation: The Influence of Anisotropy of Brain Tissue . *IEEE T Bio-med Eng*, 59:1583–1592.

Uc, E. Y. and Follet, K. A. (2007). Deep brain stimulation in movement disorders. *Semin Neurol*, 27:170–182.

van Rienen, U. (2000). *Numerical Methods in Computational Electrodynamics: Linear Systems in Practical Applications*. Springer, Berlin Heidelberg, 1st edition.

Walckiers, G., Fuchs, B., Thiran, J. P., Mosig, J. R., and Pollo, C. (2010). Influence of the implanted pulse generator as reference electrode in finite element model of monopolar deep brain stimulation. *J Neurosci Meth*, 186:90–96.

Wei, X. F. and Grill, W. M. (2009). Impedance characteristics of deep brain stimulation electrodes in vitro and in vivo. *J Neural Eng*, 6:046008.

Xiu, D. (2010). *Numerical Methods for Stochastic Computations: A Spectral Method Approach*. Princeton University Press.

Yousif, N. and Liu, X. (2009). Investigating the depth electrode-brain interface in deep brain stimulation using finite element models with graded compexity in structure and solution. *J Neurosci Meth*, 184:142–151.